

Proximity spin-orbit coupling in an armchair carbon nanotube on monolayer bismuthene.

Marcin Kurpas*

Institute of Physics, University of Silesia in Katowice, 41-500 Chorzów, Poland

(Dated: May 19, 2023)

We study spin-orbit proximity effects in a hybrid heterostructure build of a one-dimensional (1D) armchair carbon nanotube and two-dimensional (2D) buckled monolayer bismuthene. We show, by performing first-principles calculations, that Dirac electrons in the nanotube exhibit large spin-orbit coupling due to a close vicinity of bismuthene. The calculated low-energy band structures of the proximized nanotube display a strong dependence on the position of the nanotube on the substrate, similar to twist-angle dependence found in 2D heterostructures. Based on the first-principles results, we formulate an effective low-energy Hamiltonian of the nanotube and identify key interactions governing the proximity spin-orbit coupling. The proximity-induced spin splitting of Dirac cone bands is in meV range, confirming an efficient transfer of spin-orbit coupling from bismuthene to the nanotube.

I. INTRODUCTION

Two-dimensional (2D) Van der Waals heterostructures have become versatile platforms to study physical phenomena in low dimensions and promising building blocks for novel devices for quantum technologies¹⁻³. This was possible thanks to the great ease of modifying their electronic properties, for example, by the proximity effect. It allows a material to acquire new properties by stacking it on top of another material, being the donor of those properties. Graphene, for instance, is essentially free of intrinsic spin-orbit coupling^{4,5}, but can realize spin Hall states when embedded into a heterostructure with WS₂ or MoS₂⁶⁻⁹.

The effectiveness of the proximity effect to a large extent is dictated by symmetry and physics at the interface between materials. The presence of a substrate breaks most symmetries of the host material, releasing several constraints on the electron spin and symmetry-allowed spin-orbit terms. Broken space inversion symmetry leads to the emergence of Bychkov-Rashba spin-orbit coupling affecting both, spin splitting and spin texture of Bloch states^{7,10,11}. Other symmetries, such as in-plane mirror symmetry or pseudospin (sublattice) symmetry can also be broken if present, enabling additional matrix elements of spin-orbit Hamiltonian¹²⁻¹⁴.

The extent to which broken symmetry affects the electronic states depends on the amplitudes of new symmetry-allowed terms. These amplitudes result from the interface crystal potential, which reflects mutual interactions and the atomic arrangement of the host material and the substrate. In commensurate 2D heterostructures, the interface potential is lattice periodic, with the period of the supercell. Within the supercell, its shape depends on the misfit and mutual arrangement of materials composing the heterostructure. The latter can be tuned, for example, by a twist angle, giving the control over the proximity effect¹⁵⁻¹⁷.

When the host 2D material is replaced by a one-dimensional (1D) carbon nanotube, the 2D in-plane periodicity of the interface is preserved only in one direction,

say z [see Fig. 1 c)], while in the other [y in Fig. 1 c)] it is broken due to finite diameter of the nanotube. It has severe consequences for the electronic states in the nanotube. First, broken rotational symmetry of the nanotube does not protect the longitudinal (along the nanotube axis) component of the electron spin^{18,19}. Second, a rapid variation of the crystal potential in the y direction and the non-uniform distance of carbon atoms to the substrate make room for new interface effects absent in flat 2D systems²⁰.

In this paper we study such effects in an example hybrid 1D/2D heterostructure made of a (4,4) armchair carbon nanotube and buckled monolayer bismuthene²¹⁻²⁴. To accurately describe structural changes and interactions between the nanotube and bismuthene we approach the problem on the atomistic level and perform first principles calculations based on the density functional theory. We show that orbital and spin-orbital properties of the nanotube are very sensitive to the position of the nanotube on the substrate. By moving the nanotube, we induce qualitative changes in the topology and spin structure of the Dirac cone bands, similar to the twisting of graphene on transition metal dichalcogenides¹⁷. The band structures topologies resemble those of armchair carbon nanotubes in coexisting external electric and magnetic fields¹⁹. We use this resemblance as a hint in developing an effective low-energy Hamiltonian of the nanotube.

Proximity effects in carbon nanotubes have not been yet intensively studied. So far the focus has been on superconductivity²⁵, charge transfer and contact formation between nanotubes and metal surfaces^{20,26-29}, or optical properties of the CNT/GeSe heterostructure³⁰. Carbon nanotubes proximized to a superconductor have also been investigated in the context of topological states³¹⁻³⁴, but without studying the underlying proximity mechanism. Not much is known about spin properties of nanotubes combined with 2D materials or bulk surfaces. This work gives an insight into this topic and demonstrates that hybrid 1D/2D heterostructures are attractive for exploring spin-orbit proximity effects.

The paper is organized as follows. In the next section we briefly describe methodology and details of first principles calculations. In Section III we present and discuss results of the calculations and develop an effective low energy Hamiltonian for the nanotube. Section IV contains a summary and closing conclusions.

II. METHODS

First principles calculations were performed with the plane wave software package QUANTUM ESPRESSO^{35,36}. The heterostructure of CNT and bismuthene was made of 24 Bi atoms building the substrate of width 25.5 Å and 48 C atoms forming three unit cells of the (4,4) armchair nanotube. The big width of bismuthene stripe was necessary to eliminate possible bending of bismuthene at the edges of the simulation cell. To ensure the commensurability of the structure, the lattice constant of bismuthene was reduced to $a_{\text{Bi}} = 4.4$ Å, resulting in its slight compression, of about 3%, comparing to the experimental value³⁷. The lattice constant of CNT was $a_{\text{cnt}} = 2.46$ Å. A vacuum of 16 Å was introduced in the x direction (out of plane) to avoid fictitious interactions between periodic copies of the simulation cell.

The initial geometry of the heterostructure (Fig. 1 a), b)) was optimized by minimizing the internal forces acting on atom using the quasi-Newton scheme, as implemented in QUANTUM ESPRESSO, and assuming ionic minimization convergence criteria: 10^{-3} Ry/bohr for internal forces and 10^{-5} Ry/bohr for the total energy. During relaxation all atoms were free to move in all directions. Taking into account that Bi is a heavy element, we performed optimization independently for the non-relativistic and relativistic calculations, taking the output from the non-relativistic case as the initial structure for the relativistic calculation. Nevertheless, we have not found substantial differences between the two optimized structures. In both cases, the ultrasoft pseudopotentials implementing the Perdew-Burke-Ernzerhof (PBE)³⁸ version of the generalized gradient approximation (GGA) exchange-correlation functional was used, with the kinetic energy cutoff of the plane wave basis sets 48 Ry for the wave function and 485 Ry for charge density. Self consistency was achieved with $4 \times 10 \times 1$ Monkhorst-Pack grid³⁹ while for structure optimization we used a smaller grid $1 \times 4 \times 1$. All calculations were done including the semiempirical van der Waals corrections^{40,41} and the dipole correction⁴² for a proper determination of the possible energy offset.

For visualization of crystal structures we used the XCrysDen software⁴³. Fitting of the model Hamiltonian to DFT data was done with help of the least square fitting method implemented in the LMFIT library⁴⁴.

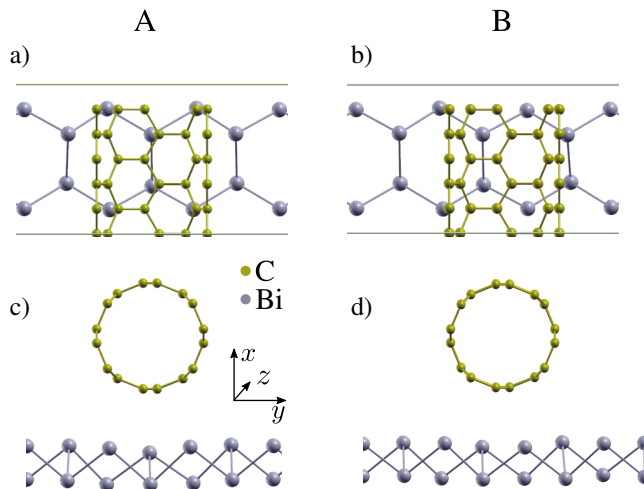


FIG. 1. Schematics of the simulated system: a metallic armchair (4,4) carbon nanotube is placed on monolayer buckled bismuthene. Depending of the position of the nanotube on bismuthene, two different configurations are realized: (a) the zigzag chain of the nanotube is in line with Bi atoms, this is labelled as the A configuration ;(b) the nanotube's bottom zigzag chain is located between two Bi atoms (B configuration). For better visibility, only C atoms closest to the substrate are drawn in (a) and (b). In c) and d) optimized crystal structures are shown.

III. RESULTS AND DISCUSSION

A. First principles results

We begin with discussing the geometry of the nanotube/bismuthene heterostructure. In Fig. 1 a),b) we show two configurations studied in this paper. The structures differ in the alignment of the nanotube with respect to the substrate. In configuration A, the lowest zigzag chain of the CNT is in line with the underlying Bi atoms, and C atoms closest to the substrate sit on top of Bi atoms (top position). Configuration B is made from A by shifting the nanotube in the y direction by half of the unit cell of bismuthene, such that the lowest zigzag chain of C atoms lies between Bi atoms (hollow position).

Different initial conditions for A and B setups lead to slightly different responses of bismuthene substrate during structure optimization. In case A, only the atomic Bi chain below the nanotube is pushed down, while in case B, two Bi chains lower their initial position [Fig. 1 c),d)]. The distances between the nanotube and the underneath Bi atom(s) are 3.28 Å and 3.15 Å for the A and B configurations, respectively. We did not notice any substantial changes to the geometry of the nanotube. Energetically the two configurations are very close to each other. The total energy of the whole system for configuration B is 16 meV lower than for A, indicating that both are similarly probable for experimental realizations.

In Fig. 2 a) we show the calculated non-relativistic band structure for the configuration A plotted along the

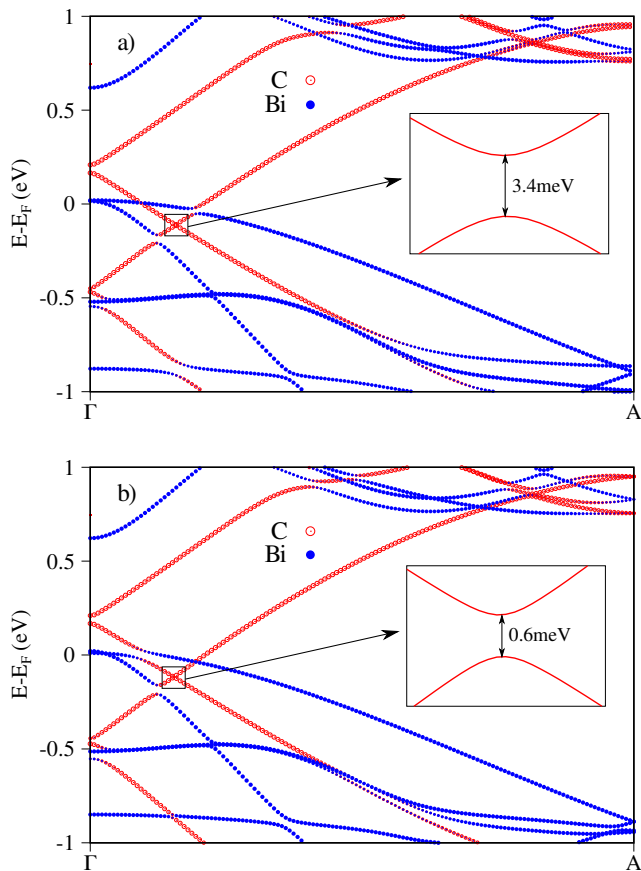


FIG. 2. Non-relativistic band structure from first principles calculations. Red color represents C electrons, blue color Bi electrons. a) the band structure for the full First Brillouin zone and A configuration; b) a close view at the region around the Dirac cone of the nanotube on the A configuration; c) same as b) but for B configuration.

ΓA line in the Brillouin zone of the nanotube. This direction corresponds to crystal momentum along the nanotube axis parallel to the armchair edge of bismuthene. Bands of the nanotube (red) are easily distinguishable. The Dirac cone lies 0.1 eV below the Fermi level due to electron doping from the substrate and is well preserved up to ± 50 meV from its center. Hybridization effects are visible on the left and right sides of the Dirac cone as anticrossings between C and Bi bands. A close look at the Dirac cone (inset in Fig. 2 a)) reveals opening a sizeable orbital energy gap $\Delta_{\text{orb}}^A = 3.4$ meV in the energy spectrum of metallic nanotube due to interaction with the substrate.

The electronic band structure for configuration B is very similar to A (Fig. 2 b)). Differences are visible in hybridization states at crystal momenta close to the position of the Dirac cone of the nanotube. The anticrossing at the Fermi energy visible to the right from the Dirac cone for A disappears and is visible to the left from the Dirac cone. A similar effect occurs at energy ≈ -0.75 eV below the Fermi level. Most striking is the

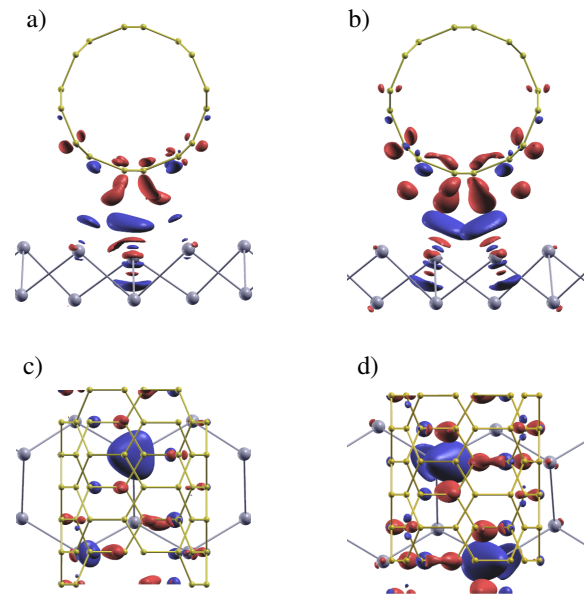


FIG. 3. Iso-surfaces of charge density at the interface of CNT and bismuthene within one unit cell: a) side view for the configuration A; b) side view for the configuration B. c), d) top-view for the A and B configurations respectively. The blue (red) color represents negative (positive) values of charge density.

reduction of the orbital gap, $\Delta_{\text{orb}}^B = 0.6$ meV, which is almost six times less than for case A.

Since only orbital effects have been considered so far, such significant differences in Δ_{orb} between the configurations should also be visible in the interface potential. Our conjecture is confirmed in Fig. 3, where we show the interface charge density iso-surfaces $\rho(\mathbf{r})_{\text{int}}$,

$$\rho(\mathbf{r})_{\text{int}} = \rho(\mathbf{r}) - \rho(\mathbf{r})_{\text{Bi}} - \rho(\mathbf{r})_{\text{cnt}}. \quad (1)$$

Here $\rho(\mathbf{r})$ is the total charge density of the full system, and $\rho(\mathbf{r})_{\text{Bi/cnt}}$ is the charge density of the slab/nanotube respectively. Qualitative differences in $\rho(\mathbf{r})_{\text{int}}$ between A and B configurations are evident. For the former, a single big charge pocket (big blue lobe in Fig. 3c)) is formed (approximately) below one C atom, while for the latter two lobes are localized below C atoms belonging to different sublattices of the nanotube (Fig. 3d)). As we will show below, details of the interface potential also strongly impact the spin-orbit coupling in the nanotube.

Relativistic effects in carbon nanotubes are much stronger than in flat graphene due to curvature-induced hopping between σ and π orbitals^{18,45–48}. In armchair nanotubes, effects of intrinsic spin-orbit coupling in the band structure are manifested by opening a spin-orbital gap at the K -point, while bands remain spin doublets, which is guaranteed by space inversion and time reversal symmetry. Theory predicts, that the value of the spin-orbital gap at the Dirac point is $\Delta_{\text{so}}^K = 0.6 \text{ meV}/d - 0.85 \text{ meV}/d$, where d is the diameter of the nanotube in nanometers^{49,50}. This is roughly two orders larger than

for graphene, for which $\Delta_{\text{so}}^{\text{K}} \approx 25 \mu\text{eV} - 40 \mu\text{eV}$ ^{4,5}. Our first principles calculations give for pristine (4,4) nanotube of diameter $d = 0.55 \text{ nm}$, $\Delta_{\text{so}}^{\text{K}} = 1.55 \text{ meV}$, in a good agreement with the above formula.

In Fig. 4 a), b) we show calculated relativistic band structures of CNT/Bi heterostructure projected onto the atomic states of Bi and C. The inclusion of SOC removes the orbital degeneracy of Bi states at the Fermi level pulling them apart by 164 meV. Spin states are also split off by energy of about 50 meV, which is unsurprising considering the sizeable atomic number of bismuth $Z=83$ and strong spin-orbit coupling in bismuthene⁵¹.

Similar to the non-relativistic case, the Dirac cone of the nanotube is well separated from Bi bands. A closer look reveals differences in the band structure topology for A and B configurations. For the former, the top valence and bottom conduction bands of the nanotube meet at the same k -point but the outer spin subbands are misaligned, leading to a pronounced asymmetry of spin splitting $\Delta_{\uparrow\downarrow}$ between the right and left movers (see inset in Fig. 4 a)). The splitting is also particle-hole asymmetric. In the hole branch states at the band maximum are split off by $\Delta_{\uparrow\downarrow} = 7 \text{ meV}$, while at the conduction band minimum $\Delta_{\uparrow\downarrow} = 4 \text{ meV}$. In both cases the values largely exceed splittings induced by a transverse external electric field. Our first principles calculations give splitting energy on the order $\approx 10 \mu\text{eV}/\text{Vnm}^{-1}$, on the same level as for graphene⁴.

The corresponding spin expectation values of Dirac cone bands are shown in Fig. 5 b)-d). Besides the S_y component, expected from the crystal potential gradient in the x direction (normal to the surface of bismuthene), also S_x is pronounced. S_z component is weak, which can be understood as a consequence of the lack of an intrinsic Zeeman field polarizing spins along the tube axis in chiral and zigzag tubes⁴⁹.

A qualitative different picture of the Dirac cone bands is seen for configuration B [see inset in Fig. 4 b)]. Instead of a vertical energy splitting of spin states we observe a horizontal shift of bands in crystal momentum, in opposite direction for each band, resulting in the emergence of two cones of similar energies but opposite spin. This is confirmed by tracing the spin texture of bands shown in Fig. 6 b)-d). For instance, the spin expectation in the band VB1 changes from 0.5 to -0.5 at the band maximum ($k \approx -0.008 \text{ nm}^{-1}$), but at $k = 0$ the two cones interchange and spin turns back towards 0.5. In contrast to case A, in configuration B, the gap between the branches significantly increases from 0.6 meV in the non-relativistic case to 2.4 meV, indicating its spin-orbital origin.

B. Effective Hamiltonian

The topology of Dirac cone bands is very similar to the energy spectrum of armchair nanotubes in coexisting transverse electric and magnetic fields^{19,52}. We exploit these similarities to build an effective model capturing es-

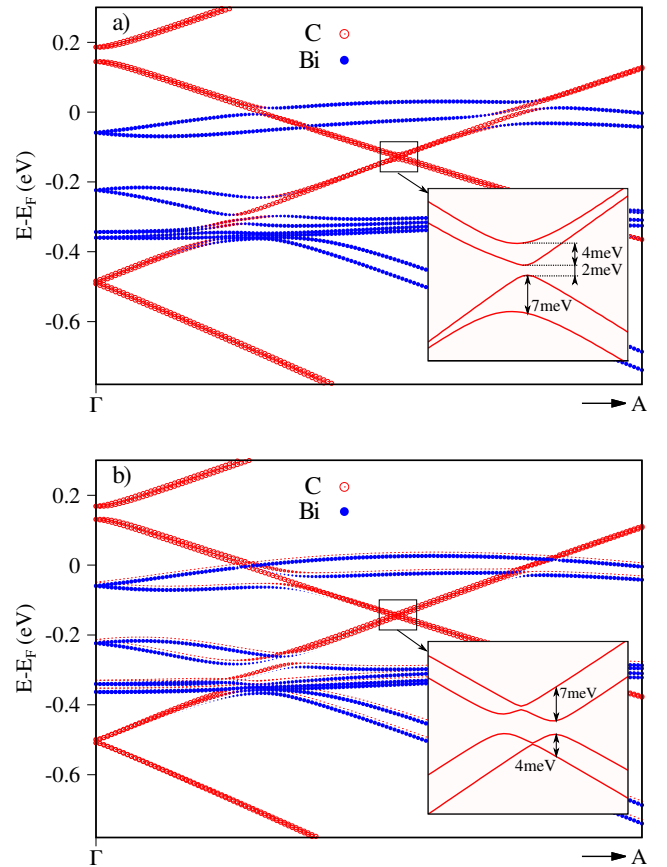


FIG. 4. Relativistic band structure from first principles projected onto C (red) and Bi (blue) atomic states. Panels a) and b) correspond to the A and B configurations, respectively. Strong repulsion and spin splitting in Bi bands modifies hybridization between states of CNT and bismuthene compared to the non-relativistic calculation.

sential features shown by first principles results. We start from the orbital Hamiltonian of an infinite pristine armchair nanotube describing linear dispersion of the Dirac cone¹⁹

$$H^{arm} = \tau \hbar v_F k \sigma_2. \quad (2)$$

Here, $\tau = \pm 1$ is the valley index, v_F is the Fermi velocity, k is longitudinal crystal momentum, and σ_2 is the Pauli matrix acting on the sublattice degree of freedom. To describe opening of the orbital gap we introduce a staggered on-site potential Δ_{st} diagonal in spin basis

$$H^{st} = \Delta_{st} \sigma_3. \quad (3)$$

The parameter Δ_{st} includes the contribution from several factors affecting the orbital gap, such as, the deformation of the nanotube and renormalization of the gap by crystal potential from the substrate. We use the orbital Hamiltonian $H^{orb} = H^{arm} + H^{st}$ to find initial values for v_F and Δ_{st} by fitting the model to the first principles energy spectrum.

Next, we add effects of spin-orbit coupling. The intrinsic spin-orbit coupling opening a spin-orbital gap in

at the K -point in pristine armchair nanotube is given by^{19,49}

$$H^{int} = \alpha S_z \sigma_1, \quad (4)$$

where S_z is the spin one-half operator with eigenvalues ± 1 , and α is a parameter defining the strength of SOC.

The interaction of the nanotube with the substrate changes the charge density profile and generates non-vanishing crystal potential gradients, or equivalently, electric fields. A static electric field in the x (stacking) direction generates the Hamiltonian¹⁹

$$H^R = \tau E_x S_y \sigma_2, \quad (5)$$

where E_x is the electric field strength in meV. This term is responsible for symmetrically splitting spin subbands in each branch of the Dirac cone and spin polarization in the y direction.

Finally, we define the time reversal-symmetric effective spin-orbit Hamiltonian H^{so} that, along with Eq. (5), will play the central role in reconstructing the first principles band structure of the nanotube

$$H^{so} = \tau \Omega_1 S_y \sigma_0 + \tau \Omega_2 S_y \sigma_3 + \Omega_3 S_y \sigma_1 + \tau \Omega_4 S_z \sigma_2. \quad (6)$$

The parameters Ω_i , $i = \{1, 2, 3, 4\}$ are amplitudes of effective spin-orbit fields. Since all symmetries of the nanotube are broken, there are no constraints on the form of terms appearing in H^{so} . Thus, any term of the product $(\mathbf{p} \times \nabla V(\mathbf{r})) \cdot \boldsymbol{\sigma}$, including H^R , is allowed, provided it does not break time reversal symmetry. However, we kept minimal number of possible terms allowing us to reconstruct the first principles energy spectrum and the spin texture.

The first term in (6) can be interpreted as a Hamiltonian of an effective magnetic field in the y direction, perpendicular to the electric field E_x and to the nanotube axis (z axis). It is sublattice even, and is similar to the Hamiltonian of the intrinsic chiral magnetic field in zigzag and chiral nanotubes, $H_Z = \tau \beta S_z \sigma_0$, where the parameter β depends of the chiral angle θ , $\beta \sim 3\theta$ ^{49,53}. For armchair carbon nanotubes $\theta = \pi/6$ giving $\beta = 0$. Here, the field polarizes spins in the direction transverse to the tube axis, thus its origin is of different nature that of H_Z . Besides modifying the energy of spin states, already split off by the electric field E_x , it introduces a spin-dependent shift in k leading to an asymmetry of spin splitting for left and right movers.

The second term in (6) describes a staggered effective magnetic field with opposite sign on the A and B sublattices (sublattice odd). As we will show, these two terms in (6), together with H^R , play a dominant role in reconstructing energy spectrum and main features of the spin texture. The remaining two terms in (6) are required for correct reconstruction of spin expectation values. They involve sublattice mixing via operators σ_1 and σ_2 , in contrast to Ω_1 , and Ω_2 , which act on a given sublattice.

The parameters of the effective model are found by least squares fitting the full Hamiltonian

$$H = H^{orb} + H^{int} + H^R + H^{so} \quad (7)$$

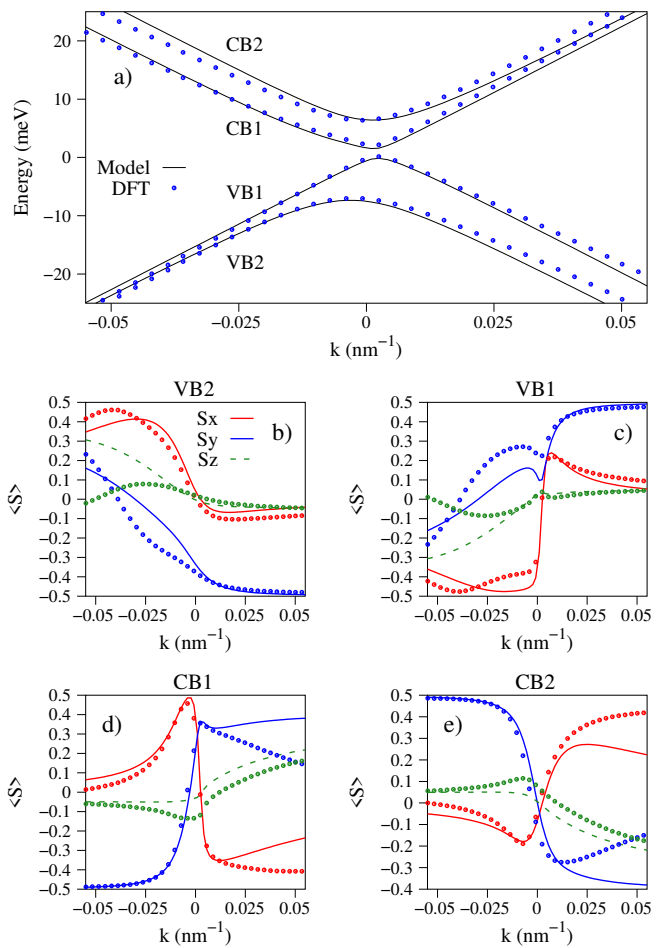


FIG. 5. Electronic properties of (4,4) armchair carbon nanotube on monolayer bismuthene for the configuration A. a) Dirac cone bands of the nanotube; b)-d) corresponding spin expectation values of bands shown in a). Dots represent first principles data while lines are results from the effective Hamiltonian (7).

to DFT data. Theoretical results superimposed on the first principles data are shown in Figs. 5 and 6, while the corresponding parameters are collected in Table I.

The overall agreement of the model with DFT data is very good. Some discrepancies in spin texture are visible in Fig. 5 a) - d), showing a rather complicated nature of the induced spin-orbit coupling in this case, probably by the nearby hybridization with the Bi bands. Looking at the values listed in Table I it is clear that the configurations A and B activate different orbital and spin-orbital fields generated by the interface crystal potential. While for the configuration A, terms with Δ_{st} , E_x , Ω_1 and Ω_2 are essential for reconstruction of the band structure and the spin texture, in the case B, the terms with E_x , and Ω_1 are sufficient to get a good agreement with DFT data. The significant value of Ω_1 in the latter case demonstrates the dominant contribution from the Zeeman-like field, which here is of extrinsic origin.

The topologies of Dirac cone bands of the nanotube

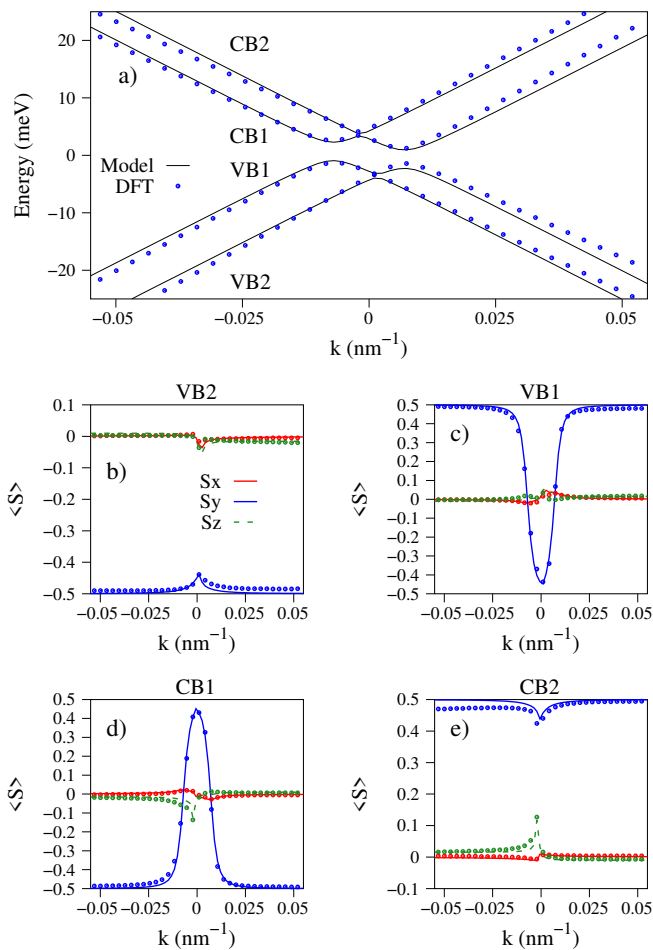


FIG. 6. Same as Fig. 5 but for the configuration B.

discussed above resemble those of graphene on transition metal dichalcogenides, where the spin-orbital proximity effect was controlled by the twist angle between the com-

ponents of the heterobilayers^{15,17,54}. Here, a similar effect is achieved by introducing a shift instead of a twist, which was shown to have marginal effects on proximity spin-orbit coupling in 2D heterostructures⁸.

IV. CONCLUSIONS

We have studied proximity spin-orbit coupling in a hybrid 1D/2D heterostructure made of an armchair carbon nanotube and buckled monolayer bismuthene. Using first-principles calculations, we have found that Dirac electrons of the nanotube are very sensitive to the interface crystal potential reflecting the atomic environment created by the substrate. We modified the latter by changing the position of the nanotube and induced qualitative changes in the topology and spin texture of Dirac cone Bloch states. These changes were triggered by a change of effective spin-orbital fields at the interface being the analogs of external magnetic and electric fields, as we showed by an effective model analysis. The proximity-induced spin-orbit coupling in Dirac cone is on meV range, much beyond the capabilities of a transverse external electric field, which demonstrates an effective transfer of spin-orbit coupling from bismuthene to the nanotube.

ACKNOWLEDGMENTS

The authors thanks M. Marganska-Lyzniak, M. Gmitra, M. Milivojević, and J. Fabian for fruitful discussions. The authors acknowledge support from the Interdisciplinary Centre for Mathematical and Computational Modelling (ICM), University of Warsaw (UW), within grant no. GA84-43. The project is co-financed by the National Center for Research and Development (NCBR) under the V4-Japan project BGapEng V4-JAPAN/2/46/BGapEng/2022.

* marcin.kurpas@us.edu.pl

- ¹ K. S. Novoselov, A. Mishchenko, A. Carvalho, and A. H. C. Neto, *Science* **353**, aac9439 (2016).
- ² I. Žutić, A. Matos-Abiague, B. Scharf, H. Dery, and K. Belashchenko, *Materials Today* **22**, 85 (2019).
- ³ A. Avsar, H. Ochoa, F. Guinea, B. Özyilmaz, B. J. van Wees, and I. J. Vera-Marun, *Rev. Mod. Phys.* **92**, 21003 (2020).
- ⁴ M. Gmitra, S. Konschuh, C. Ertler, C. Ambrosch-Draxl, and J. Fabian, *Phys. Rev. B* **80**, 235431 (2009).
- ⁵ J. Sichau, M. Prada, T. Anlauf, T. J. Lyon, B. Bosnjak, L. Tiemann, and R. H. Blick, *Phys. Rev. Lett.* **122**, 046403 (2019).
- ⁶ A. Avsar, J. Y. Tan, T. Taychatanapat, J. Balakrishnan, G. K. W. Koon, Y. Yeo, J. Lahiri, A. Carvalho, A. S. Rodin, E. C. T. O'Farrell, G. Eda, A. H. Castro Neto, and B. Özyilmaz, *Nat. Commun.* **5**, 4875 (2014).
- ⁷ M. Gmitra and J. Fabian, *Phys. Rev. B* **92**, 155403 (2015).
- ⁸ M. Gmitra, D. Kochan, P. Högl, and J. Fabian, *Phys. Rev. B* **93**, 155104 (2016).
- ⁹ C. K. Safeer, J. Ingla-Aynés, F. Herling, J. H. Garcia, M. Vila, N. Ontoso, M. R. Calvo, S. Roche, L. E. Hueso, and F. Casanova, *Nano Lett.* **19**, 1074 (2019).
- ¹⁰ Y. Bychkov and E. Rashba, *JETP Lett.* **39**, 78 (1984).
- ¹¹ W. Han, R. K. Kawakami, M. Gmitra, and J. Fabian, *Nat. Nanotechnol.* **9**, 794 (2014).
- ¹² G. Giovannetti, P. A. Khomyakov, G. Brocks, P. J. Kelly, and J. van den Brink, *Phys. Rev. B* **76**, 073103 (2007).
- ¹³ C. Weeks, J. Hu, J. Alicea, M. Franz, and R. Wu, *Phys. Rev. X* **1**, 021001 (2011).
- ¹⁴ D. Kochan, S. Irmer, and J. Fabian, *Phys. Rev. B* **95**, 165415 (2017).
- ¹⁵ Y. Li and M. Koshino, *Phys. Rev. B* **99**, 075438 (2019).

TABLE I. Parameters of the effective Hamiltonian (2) obtained by least square fitting to the first principles data.

Configuration	Δ_{st} (meV)	v_F (nm · s ⁻¹)	E_x (meV)	Ω_1 (meV)	Ω_2 (meV)	Ω_3 (meV)	Ω_4 (meV)	α (meV)
A	1.74	$6.9 \cdot 10^{14}$	-1.75	1.4	-2.6	0	-0.3	3.2
B	0.17	$6.8 \cdot 10^{14}$	0.67	3.2	-0.16	0.1	-0.07	1.6

- ¹⁶ K. Zollner, P. E. Faria Junior, and J. Fabian, Phys. Rev. B **100**, 085128 (2019).
- ¹⁷ T. Naimer, K. Zollner, M. Gmitra, and J. Fabian, Phys. Rev. B **104**, 195156 (2021).
- ¹⁸ D. Huertas-Hernando, F. Guinea, and A. Brataas, Phys. Rev. B **74**, 155426 (2006).
- ¹⁹ J. Klinovaja, M. J. Schmidt, B. Braunecker, and D. Loss, Phys. Rev. B **84**, 1 (2011).
- ²⁰ M. Hasegawa and K. Nishidate, Phys. Rev. B **83**, 155435 (2011).
- ²¹ T. Nagao, J. T. Sadowski, M. Saito, S. Yaginuma, Y. Fujikawa, T. Kogure, T. Ohno, Y. Hasegawa, S. Hasegawa, and T. Sakurai, Phys. Rev. Lett. **93**, 105501 (2004).
- ²² S. Yaginuma, K. Nagaoka, T. Nagao, G. Bihlmayer, Y. M. Koroteev, E. V. Chulkov, and T. Nakayama, J. Phys. Soc. Japan **77**, 014701 (2008).
- ²³ I. K. Drozdov, A. Alexandradinata, S. Jeon, S. Nadj-Perge, H. Ji, R. J. Cava, B. A. Bernevig, and A. Yazdani, Nat. Phys. **10**, 664 (2014).
- ²⁴ E. Aktürk, O. U. Aktürk, and S. Ciraci, Phys. Rev. B **94**, 014115 (2016).
- ²⁵ A. F. Morpurgo, J. Kong, C. M. Marcus, and H. Dai, Science **286**, 263 (1999).
- ²⁶ S. Okada and A. Oshiyama, Phys. Rev. Lett. **95**, 206804 (2005).
- ²⁷ Y. Takagi and S. Okada, Phys. Rev. B **84**, 035406 (2011).
- ²⁸ A. A. Kuzubov, E. A. Kovaleva, P. Avramov, A. V. Kuklin, N. S. Mikhaleva, F. N. Tomilin, S. Sakai, S. Entani, Y. Matsumoto, and H. Naramoto, J. Appl. Phys. **116**, 084309 (2014).
- ²⁹ Y. Liao, K. Mustonen, S. Tulić, V. Skákalová, S. A. Khan, P. Laiho, Q. Zhang, C. Li, M. R. Monazam, J. Kotakoski, H. Lipsanen, and E. I. Kauppinen, ACS Nano **13**, 11522 (2019).
- ³⁰ Y. Mao, Z. Guo, J. Yuan, and T. Sun, Nanomaterials **11**, 1565 (2021).
- ³¹ R. Egger and K. Flensberg, Phys. Rev. B **85**, 1 (2012).
- ³² J. Klinovaja, S. Gangadharaiyah, and D. Loss, Phys. Rev. Lett. **108**, 1 (2012).
- ³³ M. Marganska, L. Milz, W. Izumida, C. Strunk, and M. Grifoni, Phys. Rev. B **075141**, 1 (2018).
- ³⁴ L. Milz, W. Izumida, M. Grifoni, and M. Marganska, Phys. Rev. B **100**, 155417 (2019).
- ³⁵ P. Giannozzi, S. Baroni, N. Bonini, M. Calandra, R. Car, C. Cavazzoni, D. Ceresoli, G. L. Chiarotti, M. Cococcioni, I. Dabo, *et al.*, J. Phys.: Condens. Matter **21**, 395502 (2009).
- ³⁶ P. Giannozzi, O. Andreussi, T. Brumme, O. Bunau, M. Buongiorno Nardelli, M. Calandra, R. Car, C. Cavazzoni, D. Ceresoli, M. Cococcioni, *et al.*, J. Phys.: Cond. Mat. **29**, 465901 (2017).
- ³⁷ H. Mönig, J. Sun, Y. M. Koroteev, G. Bihlmayer, J. Wells, E. V. Chulkov, K. Pohl, and P. Hofmann, Phys. Rev. B **72**, 085410 (2005).
- ³⁸ J. P. Perdew, K. Burke, and M. Ernzerhof, Phys. Rev. Lett. **77**, 3865 (1996); **78**, 1396(E) (1997).
- ³⁹ H. J. Monkhorst and J. D. Pack, Phys. Rev. B **13**, 5188 (1976).
- ⁴⁰ S. Grimme, J. Comput. Chem. **27**, 1787 (2006).
- ⁴¹ V. Barone, M. Casarin, D. Forrer, M. Pavone, M. Sami, and A. Vittadini, J. Comput. Chem. **30**, 934 (2009).
- ⁴² L. Bengtsson, Phys. Rev. B **59**, 12301 (1999).
- ⁴³ A. Kokalj, J. Mol. Graph. Model. **17**, 176 (1999).
- ⁴⁴ M. Newville, T. Stensitzki, D. B. Allen, and A. Ingargiola, “LMFIT: Non-Linear Least-Square Minimization and Curve-Fitting for Python,” (2014).
- ⁴⁵ T. Ando, J. Phys. Soc. Japan **69**, 1757 (2000).
- ⁴⁶ F. Kuemmeth, S. Ilani, D. C. Ralph, and P. L. McEuen, Nature **452**, 448 (2008).
- ⁴⁷ S. H. Jhang, M. Marganska, Y. Skourski, D. Preusche, B. Witkamp, M. Grifoni, H. van der Zant, J. Wosnitza, and C. Strunk, Phys. Rev. B **82**, 041404 (2010).
- ⁴⁸ G. A. Steele, F. Pei, E. A. Laird, J. M. Jol, H. B. Meerwaldt, and L. P. Kouwenhoven, Nat. Comm. **4**, 1 (2013).
- ⁴⁹ W. Izumida, K. Sato, and R. Saito, J. Phys. Soc. Japan **78**, 074707 (2009).
- ⁵⁰ J. Zhou, Q. Liang, and J. Dong, Phys. Rev. B **79**, 195427 (2009).
- ⁵¹ M. Kurpas, P. E. F. Junior, M. Gmitra, and J. Fabian, Phys. Rev. B **100**, 125422 (2019).
- ⁵² W. DeGottardi, T.-C. Wei, and S. Vishveshwara, Phys. Rev. B **79**, 205421 (2009).
- ⁵³ J. S. Jeong and H. W. Lee, Phys. Rev. B **80**, 1 (2009).
- ⁵⁴ A. David, P. Rakyta, A. Kormányos, and G. Burkard, Phys. Rev. B **100**, 085412 (2019).